Arabian Journal for Science and Engineering
https://doi.org/10.1007/s13369-018-3187-1

RESEARCH ARTICLE - MECHANICAL ENGINEERING

Dynamic Characterization of a Bistable Energy Harvester Under Gaussian White Noise for Larger Time Constant

Sovan Sundar Dasgupta[1] · Vasudevan Rajamohan[2] · Abhishek Kumar Jha[1]

Received: 6 September 2017 / Accepted: 19 March 2018

Abstract
In this paper, the system parameters of a nonlinear bistable energy harvester excited by Gaussian white noise was investigated. Using Fokker–Planck–Kolmogorov equation, the probability distribution functions of displacement and velocity of the oscillator are obtained. The effect of various system parameters on the probability distributions of displacement and velocity of the oscillator and the mean square of the output voltage are investigated when the time constant of the piezoelectric circuit takes a larger value to achieve maximum voltage gain. The maximum peak values of the joint probability distribution of displacement and velocity of the oscillator decrease with the larger values of noise strength. The effect of parameters of bistable potential function on mean square of output voltage was also investigated. The system equations are numerically solved and mean square value of output voltage is numerically estimated and is seen to be increased as noise intensity increases and decreased as viscous damping increases. The result also shows that better power output can be achieved when the time constant takes larger value.

Keywords Energy harvester · Bistable · Gaussian white noise · Time constant · Probability distribution function · Potential function

1 Introduction

Over the last two decades, research on energy harvesting methods and technologies has received growing attention [1–3]. The motivation in vibration-based energy harvesting is to power micro- and nanoelectronic devices such as wireless sensors and actuators through electrical energy converted from mechanical/vibrational energy capturing from several vibrating structures. It acts as an alternative power source, provides a means of extending the battery life of remote sensors and actuators in industrial, commercial and medical applications. Other applications include, remote corrosion monitoring systems, implantable devices and remote patient monitoring, structural monitoring, radio-frequency identification (RFID), low cost and low-powered electronics, nanogenerators and equipment monitoring [2,3].

✉ Sovan Sundar Dasgupta
sovan@vit.ac.in

[1] School of Mechanical Engineering, VIT, Vellore, India

[2] Centre for Innovative Manufacturing Research (CIMR), VIT, Vellore, India

Williams and Yates [4] described three basic vibration-based energy harvesters, as electromagnetic [5], electrostatic [6] and piezoelectric [7,8]. Traditionally, an energy harvester is based on resonant tuning of a linear mechanical oscillator [9]. However, linear designs suffer from a critical shortcoming in their operational concept. Specifically, their performance is enhanced only in a small frequency bandwidth where the excitation frequency is very close to the fundamental frequency of the generator (resonance conditions). But due to small variation of excitation frequency from resonance condition, performance of these harvesters can dramatically decrease.

To circumvent this issue, recently nonlinearity is purposefully introduced into the system to increase the operating frequency range and enhance its performance [10,11]. In recent years, many research papers showed that the nonlinear piezoelectric structures were more effective for broadband energy harvesting. The experimental results of Ferrari et al. [12] and Erturk and Inman [13] showed that the bistable system could produce a remarkable improvement in output power over a wider bandwidth. Friswellet et al. [14] studied the energy harvesting efficiency of a vertical cantilever beam with a tip mass when excited by horizontal excitation. These

Published online: 28 March 2018

experiments showed that bistable energy harvester (BEH) is more effective over a broad frequency range. In practice, many structures realize bistability by magnetic attraction, magnetic repulsion or material properties.

The performance of bistable piezoelectric energy harvester could be enhanced further if the system is excited by random motions. Cotton, Vocca and Gammaitoni [10] found that for a certain intensity of random excitation, a well-designed bistable harvester could tremendously improve the output power. Litak et al. [15] simulated the dynamic response of BEH driven by random excitation and showed that the energy harvested from a bistable device was the most efficient for a certain range of noise intensity. Daqaq [16] investigated theoretically a BEH under Gaussian white and exponentially correlated noise and pointed out that bistable harvester is not always preferable to monostable harvester. Kumar et al. [17] proved Daqaq's conclusion through finite element method solving the Fokker–Planck–Kolmogorov (FPK) equation and gave the joint probability distribution functions (PDF) of response.

Usually piezoelectric circuit of a bistable energy harvester behaves like a low-pass filter unless the time constant (τ_p) tends to have a very large value. Making it as a high-pass filter, i.e., $\tau_p \to \infty$, output power can be enhanced. Based on this approach, Zhu [18] investigated stationary statistical properties of nonlinear energy harvesting system under the high-pass filter. The effects of the relevant system parameters on the stationary probability distribution and the mean of the square of the output electrical voltage are discussed. Even though the effect of the system parameters of the BEH on the output power and mean square value of output voltage should be studied numerically for the quick estimation of the harvester's performance.

The current paper endeavors to investigate, the effect of various system parameters on the PDF of displacement and velocity of a BEH under Gaussian white noise. In general, a source of mechanical energy (i.e., ambient mechanical vibration, water wave, etc.) can be described in terms of displacement, velocity or acceleration spectrum. Randomness is introduced through the excitation signal and is characterized by a given spectrum, i.e., a given amplitude for each harmonics the relative phase between is unknown and can be modeled as a uniformly distributed random variable. White noise is a random signal with constant power spectral density. A single realization of white noise is a random shock. If the bandwidth of excitation is sufficiently large than that of the harvester's then a random excitation can be safely considered to be white noise.

The influence of system parameters on the mean square of the output voltage is also studied when the time constant (τ_p) of the piezoelectric circuit takes a larger value (i.e., $\tau_p \to \infty$) to achieve a maximum voltage gain. The results are in good agreement with Zhu [18]. In addition, the effect of system parameters on the joint PDF using contour plots has been discussed. Finally, numerical simulation is carried out on the system's set of nonlinear differential equations and the effect of noise intensity and other coupling parameters on the response; also, mean square of output voltage and the output power have been investigated. It is shown that the amplitude of the response of the BEH increases with increase in the noise intensity. Mean square value of output voltage increases as noise intensity increases and decreases at higher values of viscous damping. The variation of mean square value of output voltage with time for different values of coupling parameters of the piezoelectric circuit is also obtained. Power of the bistable harvester increases with larger values of time constant.

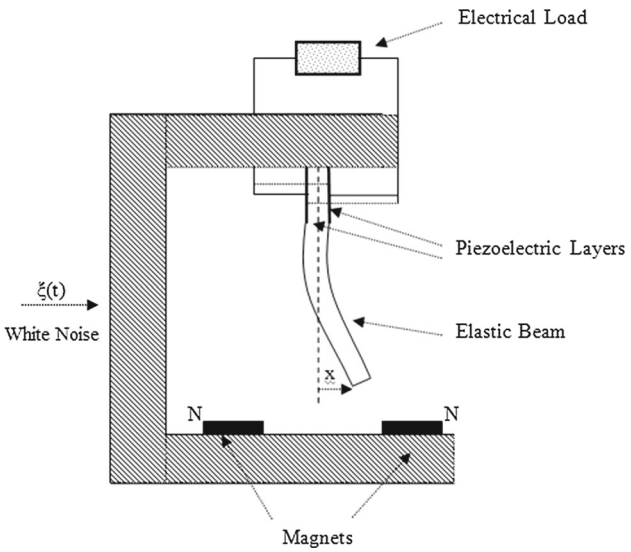

Fig. 1 Schematic diagram of a bistable piezoelectric energy harvester subjected to white noise

2 Governing Equation of Bistable Energy Harvester (BEH) Model and Response Statistics from FPK Equation

A schematic diagram of a bistable piezo-electric energy harvester (BEH) is considered for the present analysis.

A cantilever beam is fixed at one end with piezo-electric patches (i.e., bimorph) subjected to white noise as shown in Fig. 1. Near the free end of the beam, two magnets are placed to produce a repelling force in between thus creating two potential wells with two different stable equilibrium positions. Thus the beam switches between the two equilibrium positions to yield bistable effect.

Let us consider a generic piezoelectric BEH whose dynamics can be represented by a following set of coupled equations [11]:

$$\ddot{x} + \gamma \dot{x} - \frac{\mathrm{d}U(x)}{\mathrm{d}x} + \kappa_v V = \xi(t), \tag{1}$$

$$\dot{V} + \frac{V}{\tau_p} - \kappa_c \dot{x} = 0, \tag{2}$$

The physical backgrounds of different parameters are stated as follows:

$$\kappa_v = \omega_n^2 d_{33}, \quad \kappa_c = m_{eq} d_{33} \omega_n^2 / C_p, \omega_n^2 = K/m_{eq},$$
$$K = 3EI/L^3, m_{eq} = \rho AL \text{ and } \tau_p = RC_p.$$

The variables and parameters used in Eqs. (1) and (2) are defined in Table 1.

The Gaussian white noise $\xi(t)$ applied as stochastic excitation has the following statistical properties:

$$\left.\begin{aligned} &E[\xi_i(t)] = 0, \\ &E\left[\xi_i(t)\,\xi_i(t')\right] = 2D_i\delta(t-t'), \\ &E\left[\xi_i(t)\,\xi_j(t')\right] = 2\lambda_{ij}\sqrt{D_i D_j}\,\delta(t-t'), \quad (i \neq j) \end{aligned}\right\} \tag{3}$$

where E denotes the expected value of response statistics, D is noise intensity, λ_{ij} is the correlation between D_i and D_j and δ is Dirac-delta function.

The bistable potential function $U(x)$ can be defined as:

$$U(x) = -\frac{1}{2}ax^2 + \frac{1}{4}bx^4 + U_b, \tag{4a}$$

where two degenerate minima of the bistable potential located at $x_m = \pm(a/b)^{1/2}$ and the potential barrier height is given by $U_b = \frac{a^2}{4b}$ (as shown in Fig. 2b) and also the noise intensity is much smaller than the barrier height, i.e., $D \ll U_b$. The potential function $(U(x))$ is symmetrical and bistable when $a > 0$ and monostable for $a < 0$. Hardening response and softening responses are observed for $b > 0$, and $b < 0$, respectively. "a" and "b" represent the linear and nonlinear cubic stiffness terms, respectively. From the physical point of view, potential can be approximately written as:

$$U(x) = \frac{1}{2}kx^2 + \frac{\mu_0}{2\pi}\left(\frac{M_1 M_2}{\left(x^2 + d_0^2\right)^{3/2}}\right) \tag{4b}$$

where k is the spring constant, μ_0 is the vacuum permeability, M_1, M_2 are the effective magnetic moments and d_0 is the relative distance between tip of the beam and magnets [10]. The second term of RHS of Eq. (4b) represents a magnetic force-based potential. When d_0 is large, the cantilever beam behaves like a linear oscillator, and when d_0 gets smaller the cantilever behaves like a nonlinear oscillator and the potential becomes bistable.

Performing the transform $\dot{x} = y$, Eqs. (1) and (2), respectively, can be written in the following state-space form:

$$\dot{x} = y, \tag{5}$$

$$\dot{y} = -\gamma y + \frac{dU}{dx} - \kappa_v V + \xi(t), \tag{6}$$

$$\dot{V} = \kappa_c y - \frac{V}{\tau_p}. \tag{7}$$

The Fokker–Planck–Kolmogorov (FPK) equation for the probability distribution function (PDF) $P(x, y, V, t)$ of the displacement (x), oscillator velocity (y) and voltage (V) is given by

$$\left.\begin{aligned} \frac{\partial P(x,y,V,t)}{\partial t} = &-\frac{\partial(yP(x,y,V,t))}{\partial x} - \frac{\partial\left(\left(-\gamma y + \frac{dU}{dx} - \kappa_v V\right)P(x,y,V,t)\right)}{\partial y} \\ &-\frac{\partial\left(\left(\kappa_c y - \frac{V}{\tau_p}\right)P(x,y,V,t)\right)}{\partial V} + D\frac{\partial^2 P(x,y,V,t)}{\partial y^2} \end{aligned}\right\} \tag{8}$$

subjected to the boundary condition, $P(-\infty, t) = P(\infty, t) = 0$.

Upon solving Eq. (8) for $P(x, y, V, t)$, the response statistics can then be obtained via

$$E\left[\prod_{i=1}^{3} x_i^{k_i}\right] = \int_{-\infty}^{\infty}\int_{-\infty}^{\infty}\int_{-\infty}^{\infty}\prod_{i=1}^{3} x_i^{k_i} P(x, y, V, t)\mathrm{d}x\mathrm{d}y\mathrm{d}V, \tag{9}$$

where $x_1 = x, x_2 = y, x_3 = V$ and $k_i = 0, 1, 2, \ldots$.

3 Reduced Form of FPK Equation and Response Statistics for Larger Time Constant

Basically the piezoelectric dynamics represented by Eq. (7) is a linear first-order low-pass filter with oscillator velocity y and voltage V as input and output, respectively. It is extremely difficult to get a closed form solution of Eq. (8) based on some given values of noise strength and other relevant system parameters. In order to maximize the output voltage, it is assumed that the time constant of the piezoelectric dynamics takes a larger value from mathematical point of view, and it acts as a first-order high-pass filter with cutoff frequency $(\omega_c = 1/\tau_p)$.

In Eq. (7), when $\tau_p \to \infty$, one may get, $\dot{V} = \kappa_c y = \kappa_c \dot{x}$, combining it with Eqs. (5) and (6) the modified state-space form can be written as:

$$\dot{x} = y, \tag{10}$$

$$\dot{y} = -\gamma y + \frac{\mathrm{d}U}{\mathrm{d}x} - \kappa_v \kappa_c x + \xi(t). \tag{11}$$

Table 1 Different parameters and their descriptions

Parameter	Description
x	Displacement of the oscillator
V	Value of the output voltage converted by energy harvesting
γ	Linear viscous friction coefficient
κ_v	The converse piezoelectric effect, coupling coefficient that relates the oscillation to the voltage (V)
κ_c	The direct piezoelectric effect, coupling constant of the piezoelectric sample
ω_n	Natural frequency
d_{33}	Piezoelectric constant
$\xi(t)$	Environmental excitation, stochastic in nature, modeled by Gaussian white noise (Fig.2 (a))
m_{eq}	Equivalent mass of the beam
C_p	Capacitance of the piezo-electric element
τ_p	Time constant of piezo-electric dynamics
R	Resistive load
K	Linear stiffness term
E	Young's modulus
I	Area moment about the neutral axis
L	Length of the beam
ρ	Mass density of the beam material
A	cross-sectional area

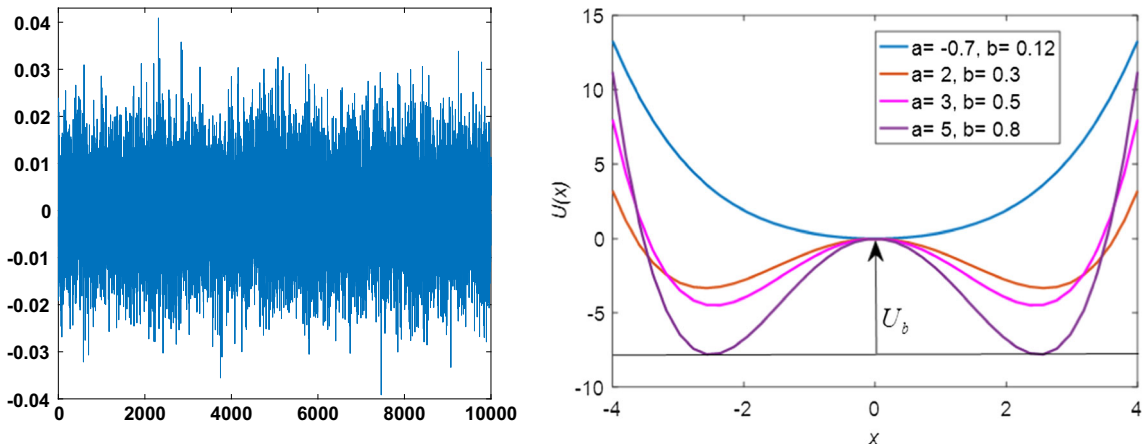

(a) **(b)**

Fig. 2 **a** Gaussian white noise for 10^4samples with zero mean and noise intensity $(D) = 0.01$. **b** Potential $(U(x))$ for different a and b values

The reduced form of FPK equation corresponding to Eqs. (10) and (11) may be expressed as

$$\left.\begin{aligned} &\frac{\partial P(x,y,t)}{\partial t} = -\frac{\partial (yP(x,y,t))}{\partial x} - \frac{\partial\left(\left(-\gamma y+\frac{dU}{dx}-\kappa_v\kappa_c x\right)P(x,y,t)\right)}{\partial y} \\ &+D\frac{\partial^2 P(x,y,t)}{\partial y^2} \\ &P(-\infty,t) = P(\infty,t) = 0 \end{aligned}\right\} \quad (12)$$

Since steady-state response statistics are of particular relevance for energy harvesting, the attention has been focused on obtaining the stationary solutions of Eq. (12). In stationary case, by making $\frac{\partial P(x,y,t)}{\partial t} = 0$ and using the modified state-space form of Eq. (11), the Eq. (12) is reduced to the following form:

$$\frac{\partial (yP(x,y))}{\partial x} + \frac{\partial\left(\left(-\gamma y + \frac{dU}{dx} - \kappa_v\kappa_c x\right)P(x,y)\right)}{\partial y} = D\frac{\partial^2 P(x,y)}{\partial y^2}. \quad (13)$$

The Eq. (13) admits the following stationary solution:

$$P_{st}(x,y) = A_1 \exp\left[-\frac{\gamma}{D}\left(-\frac{1}{2}\kappa_v\kappa_c x^2 + U(x)\right)\right] A_2 \exp\left(-\frac{c}{2D}y^2\right) = P_{st}(x)\,P_{st}(y), \quad (14)$$

where $A_1^{-1} = \int_{-\infty}^{\infty} \exp\left[-\frac{\gamma}{D}\left(-\frac{1}{2}\kappa_v\kappa_c x^2 + U(x)\right)\right]\mathrm{d}x$ and $A_2^{-1} = \int_{-\infty}^{\infty} \exp\left(-\frac{\gamma}{2D}y^2\right)\mathrm{d}y$.

The resulting joint PDF can be factored into a separable form, i.e., $P_{st}(x, y) = P_{st}(x)\, P_{st}(y)$, so that displacement (x) and velocity (y) can be treated as two independent random variables. Putting the potential function $U(x)$ into the $P_{st}(x)$ from the Eq. (4), $P_{st}(x)$ may be rewritten as,

$$P_{st}(x) = \exp\left[-\frac{\gamma}{D}\left(-\frac{1}{2}(a + \kappa_v\kappa_c)\, x^2 + \frac{1}{4}bx^4\right)\right]. \quad (15)$$

The mean square values of the displacement (x) and the velocity of the BEH(y) are given by

$$E\left[x^2\right] = \left\langle x^2\right\rangle = \int_{-\infty}^{\infty}\int_{-\infty}^{\infty} x^2 P_{st}(x, y)\,\mathrm{d}x\mathrm{d}y \quad (16)$$

and

$$E\left[y^2\right] = \left\langle y^2\right\rangle = \int_{-\infty}^{\infty}\int_{-\infty}^{\infty} y^2 P_{st}(x, y)\,\mathrm{d}x\mathrm{d}y. \quad (17)$$

The evaluation of integral of Eqs. (16) and (17) using Bessel function are shown in "Appendix".

Using the relation $V = \kappa_c x$ in conjunction with Eq. (16), the expected mean square voltage $E\left[V^2\right]$ can be written as:

$$E\left[V^2\right] = \left\langle V^2\right\rangle = \kappa_c^2 E\left[x^2\right] = \kappa_c^2 \int_{-\infty}^{\infty}\int_{-\infty}^{\infty} x^2 P_{st}(x, y)\, dxdy. \quad (18)$$

4 Results and Discussion

At first, the effect of noise intensity (D) on the stationary PDF of x, i.e., $P_{st}(x)$ has been investigated for the chosen system parameters such that:$\gamma = 0.01, \kappa_v = 0.2, \kappa_c = 1, a = 2, b = 6$. Stationary PDF of displacement (x) shown in Fig. 3a for different noise intensities has two peaks structure, distributed symmetrically about the origin, the smaller the value of D is, the larger peaks would exhibit, i.e., it reduces the stability of the system. Figure 3b shows the effect of viscous damping coefficient (γ) on the stationary PDF of displacement, i.e., $P_{st}(x)$ for the same set of system parameters. Similar to the previous results shown in Fig. 2a, $P_{st}(x)$ exhibits two peaks structure, symmetrical about left and right of the origin, respectively, but instead of diminishing, peak height tends to increase as γ increases; thus, the stability of the system is enhanced, i.e., damping increases stability. On the contrary, on increasing noise intensity (D) stability decreases as peak reduces as shown in Fig. 3a.

Figure 3a, b exhibits the effect of noise intensity (D) and viscous damping coefficient (γ) on the PDF of velocity (y), i.e., $P_{st}(y)$ respectively. In Fig. 4a, the stationary PDF of velocity (y) exhibits single peak structure and the peak value decreases as the noise intensity (D) increases. On the contrary, $P_{st}(y)$ the peak value decreases as the viscous damping increases (γ). These results are in good agreement with Zhu [18].

Figure 5a, b exhibits the effect of coefficients of the bistable potential function (i.e., a, b) and coupling parameters (κ_v, κ_c) on the mean square value of voltage $\left(\left\langle V^2\right\rangle\right)$ obtained from Eq. (18), respectively. From Fig. 4a, it is clear that $\left(\left\langle V^2\right\rangle\right)$ is a monotonically increasing function of "a" when $\gamma = 0.1$, $D = 0.5, \kappa_v = 2$ and $\kappa_c = 0.5$ but $\left(\left\langle V^2\right\rangle\right)$ increases with smaller "b."

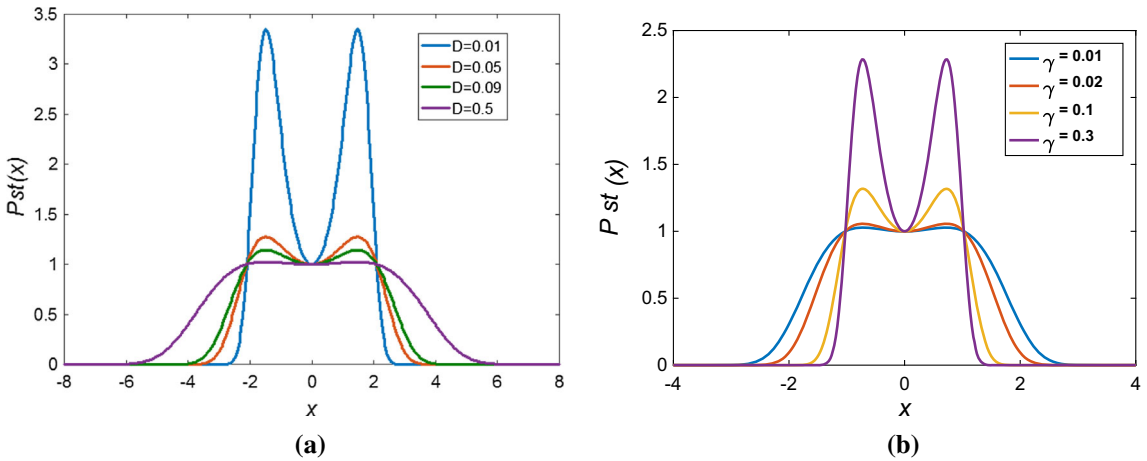

Fig. 3 **a** The effect of noise intensity (D) on the variation of stationary PDF $P_{st}(x)$ with displacement (x) of the oscillator. **b** The effect of viscous damping (γ) on the variation of stationary PDF $(P_{st}(x))$ with displacement (x) of the oscillator

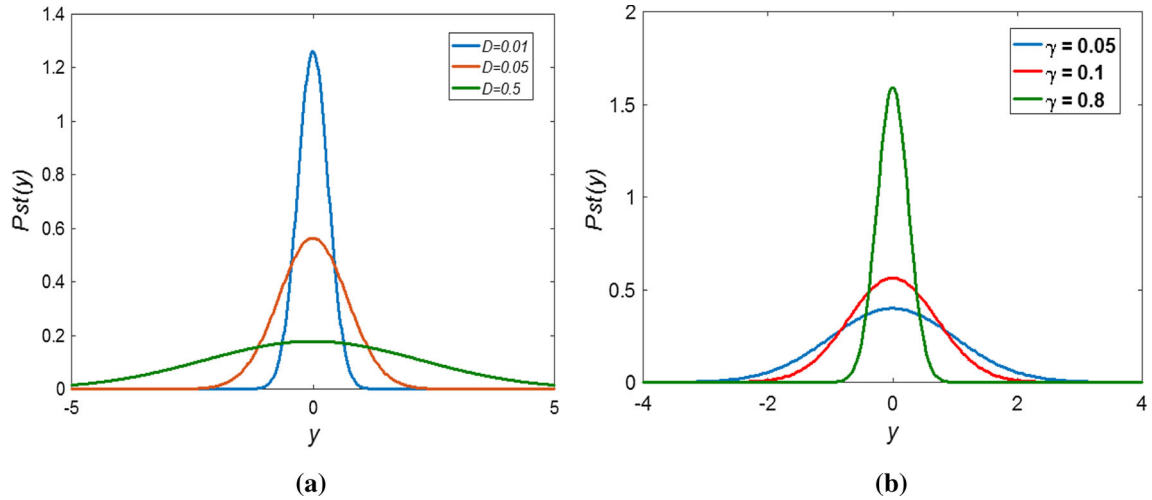

Fig. 4 **a** The effect of noise intensity D on the variation of stationary PDF $P_{st}\,(y)$ with velocity (y) of the oscillator. **b** The effect of viscous damping (γ) on the variation of stationary PDF $P_{st}\,(y)$ with velocity (y) of the oscillator

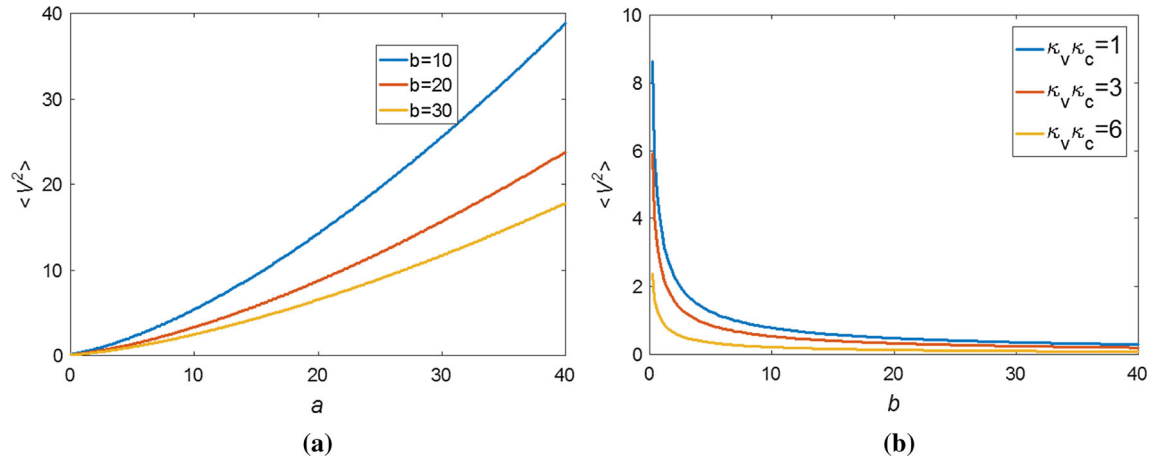

Fig. 5 **a** Variation of mean square of output voltage $\langle V^2 \rangle$ as a function of a when $\gamma = 0.1$, $D = 0.5$, $\kappa_v = 2$ and $\kappa_c = 0.5$. **b** Variation of the mean square of output voltage $\langle V^2 \rangle$ as a function of b when $\gamma = 0.01$, $D = 0.05$, $\kappa_v = 2\kappa_c = 0.5$

In Fig. 6, there exists a critical bifurcation distance, d_C, if $d_0 > d_C$ the system becomes bistable even with low intensity the two region rise together at just above d_C. For $d_0 < d_C$, the system becomes monostable.

The joint stationary PDF $P_{st}\,(x, y)$ of the displacement (x) and velocity (y) for $\gamma = 0.5, \kappa_v = 0.1, \kappa_c = 1, a = 2, b = 4$ and for different values of noise intensities $(D = 0.01, D = 0.08)$ are shown in Figs. 6a and 7a, respectively. At low values of noise intensity $D = 0.01$, the joint PDF shows two sharp peaks around two equilibrium points of the oscillator exhibiting some nonlinear interaction between the oscillator itself and the random excitation.

The corresponding contour plot as shown in Fig. 6b exhibits that they are very much similar to the phase plot of the deterministic oscillator with a strong tendency to remain near the two equilibrium points of the oscillator with bistable potential. As the noise intensity increases (i.e., D = 0.08), (Fig. 7a) the sharp bimodal peaks in the joint PDF tend to flatten and begin to merge such that owing to enhanced nonlinear interaction such that the system response has a propensity to jump from one potential well to another as shown in the corresponding contour plot (Fig. 7b). Similar observations were reported by Kumar et. al. [17] using different values of system parameters. Looking at the effect various viscous damping ($\gamma = 0.05, \gamma = 0.08$) on the joint PDF of displacement (x) and velocity (y) $P_{st}\,(x, y)$ for $D = 0.5\kappa_v = 0.1, \kappa_c = 1, a = 1.5$ and $b = 0.1$ shown in Figs. 8a and 9a, it is observed that at low viscous damping ($\gamma = 0.05$), two sharp bimodal structure of joint PDF around two equilibrium points as shown in contour plot in Fig 8b and at high value ($\gamma = 0.08$), these two peaks tend to merge showing strong nonlinear interaction of response and excitation leading to a jump from one poten-

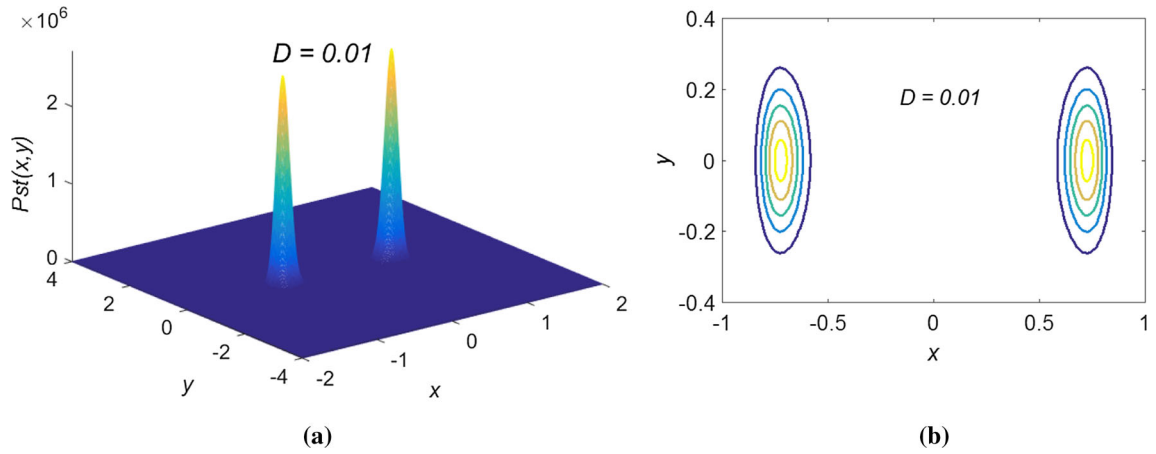

Fig. 6 **a** Variation of joint PDF of the BEH when $D = 0.01$. **b** Contour plot of joint PDF of BEH when $D = 0.01$.

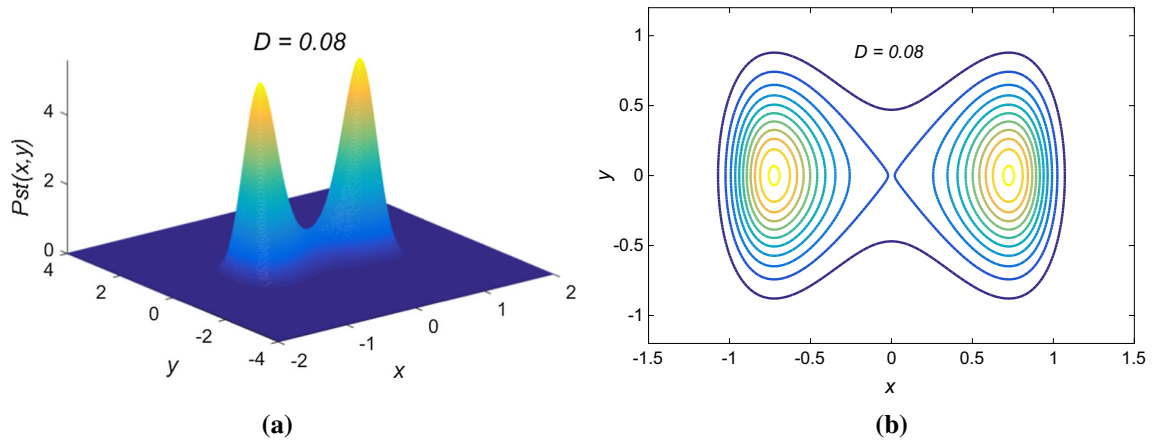

Fig. 7 **a** Joint PDF of the BEH when $D = 0.08$. **b** Contour plot of joint PDF for BEH when $D = 0.08$

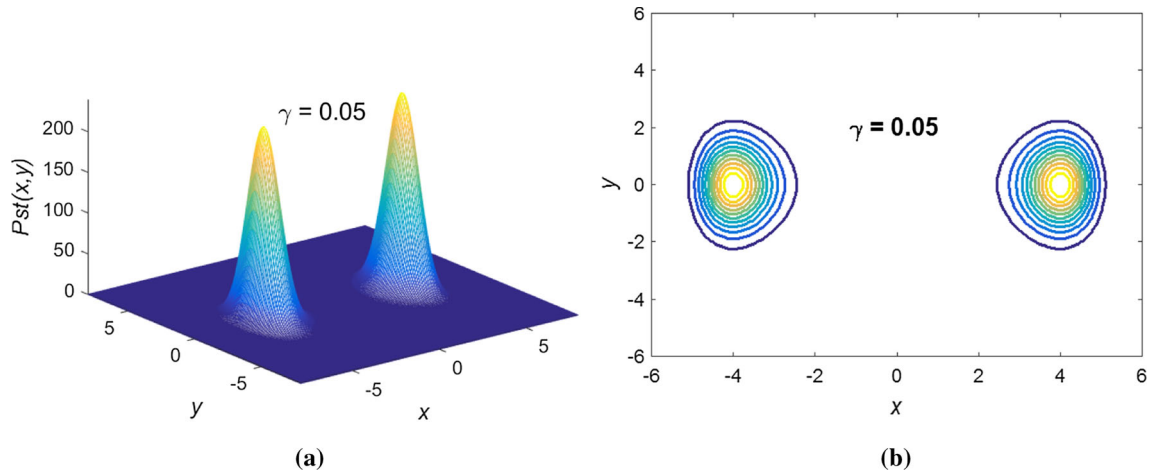

Fig. 8 **a** Joint PDF of the BEH when viscous damping $(\gamma) = 0.05$. **b** Contour plot of joint PDF for BEH when viscous damping $(\gamma) = 0.05$

tial well to another as shown in the contour plot in Fig. 9b which are very much similar to the case of noise intensity (D).

Finally, the electro-mechanically coupled Eqs. (1) and (2) are solved numerically with initial conditions $(x = 0, y = 0)$ with the help of Runge–Kutta method using ode45 solver to

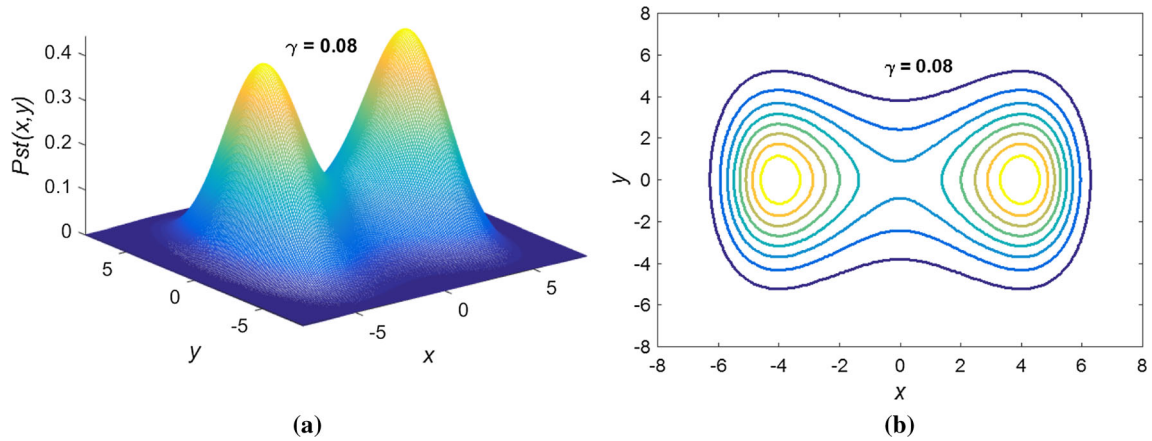

Fig. 9 **a** Joint PDF of the BEH when viscous damping $(\gamma) = 0.08$. **b** Contour plot of joint PDF for BEH when viscous damping $(\gamma) = 0.08$

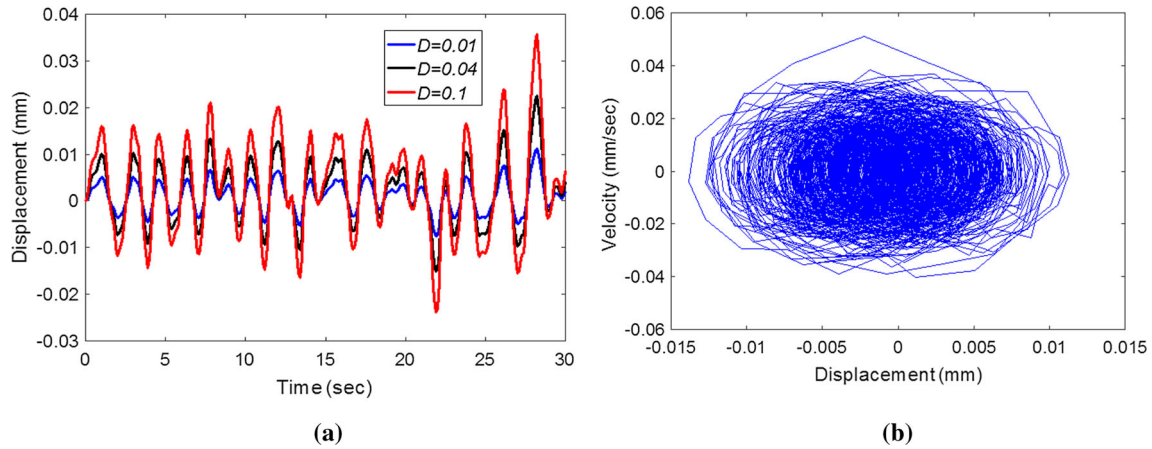

Fig. 10 **a** Dynamic response (x) with time for two values of D when $a = 1, b = 6, \gamma = 0.6, t_p = 2$ s, $\kappa_v = 200$ and $\kappa_c = 0.06$. **b** Phase portrait of the energy harvester when $a = 1, b = 6, \gamma = 0.6, D = 0.02, t_p = 2$ s, $\kappa_v = 4$ and $\kappa_c = 5$

study the effect of various system parameters on harvester's performance. Figure 10a shows the displacement response of the harvester for the chosen system parameters: $a = 1, b = 6, \gamma = 0.6, t_p = 2$ s, $\kappa_v = 200$ and $\kappa_c = 0.06$ with different values of noise intensity (D).

The amplitude of the response (x) also increases as the noise intensity (D) increases. The phase portrait of the energy harvester is shown in Fig. 10b in which orbit fills out a section of the phase plane in a complicated manner.

The mean square of output voltage $\langle V^2 \rangle$ is obtained numerically and shown in Fig. 11a, b for different noise intensities (D) and viscous damping (γ), respectively. The mean square value of output voltage $(\langle V^2 \rangle)$ is seen to be increased as the noise intensity (D) increases and viscous damping (γ) decreases as shown in Fig. 11a, b respectively.

In Fig. 12a, the variation of mean square of output voltage with time is shown for different κ_v & κ_c values. In Fig. 12b, the increasing nature of output power of the piezoelectric circuit with increase in time constant (t_p) is shown.

5 Conclusions

In this study, the effect of system parameters on the steady-state probability distribution function of a nonlinear BEH excited by Gaussian white noise has been investigated analytically when the time constant of the piezoelectric circuit becomes very large. In addition, the electro-mechanically coupled system equations were solved numerically to predict the effect of the system parameters on response, mean square value of the output voltage and power.

From the analytical and numerical investigation, the following conclusion can be drawn:

(1) Peaks of displacement PDF and velocity PDF of the harvester diminish as noise intensity increases. It reduces the stability of the system. On the contrary, peak height of both the PDFs increase as viscous damping increases, i.e., it enhances the stability of the system output.

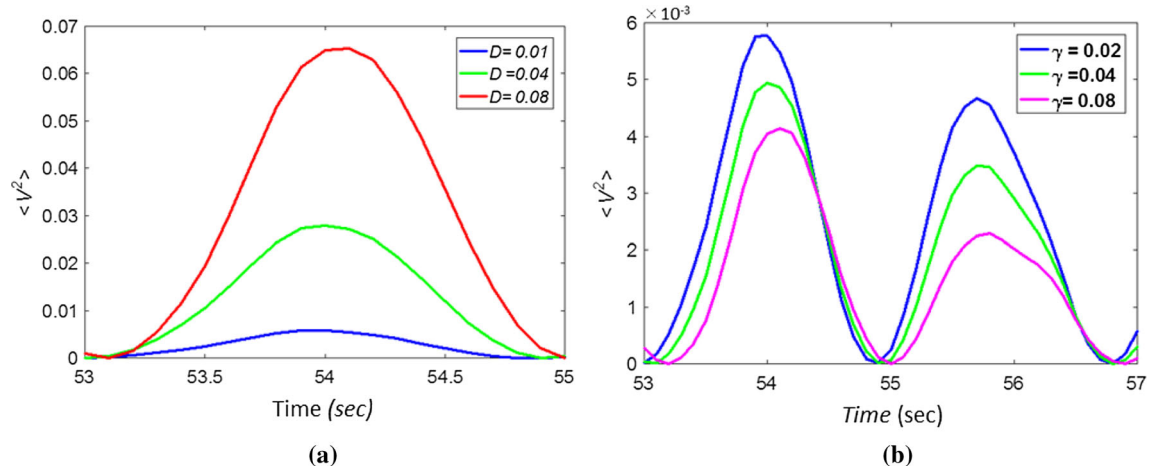

Fig. 11 **a** The mean square of output voltage $\langle V^2 \rangle$ as a function of t for various D when $\gamma = 0.02$, $R = 1\Omega$, $t_p = 2$ s, $\kappa_v = 0.2$ and $\kappa_c = 2$. **b** The mean square of output voltage $\langle V^2 \rangle$ as a function of t for different values of γ when $D = 0.04$, $R = 1\Omega$, $t_p = 2$ s, $\kappa_v = 0.2$ and $\kappa_c = 2$

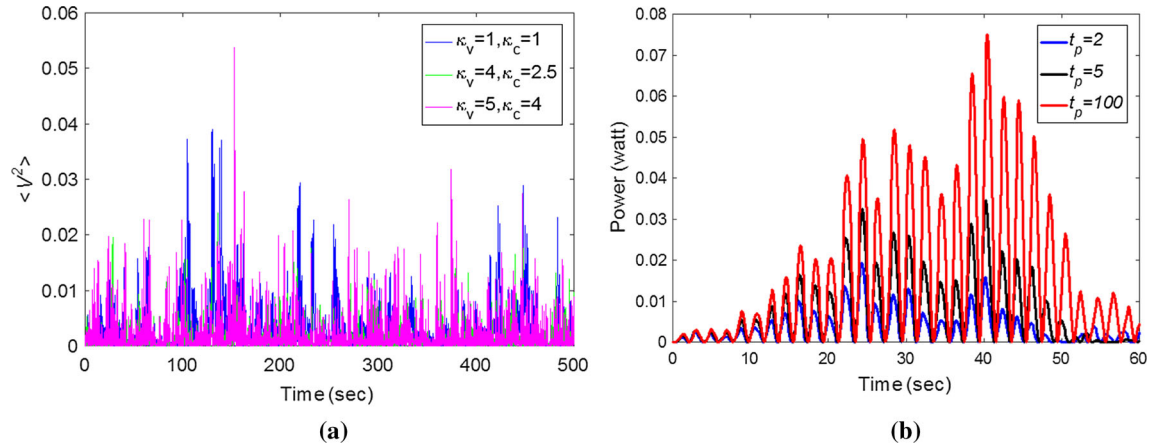

Fig. 12 **a** Time history of mean square of output voltage $(\langle V^2 \rangle)$ for different values of κ_v, κ_c when $R = 2\Omega$, $a = 2$, $b = 0.6$, $D = 0.4$, $t_p = 0.5s$ and $\gamma = 0.02$. **b** Variation of power with time for different time constants (t_p) when $D = 0.4$, $\gamma = 0.02$, $R = 2\Omega$, $a = 2$, $b = 0.6$, $\kappa_v = 1$ and $\kappa_c = 0.6$.

(2) Mean square of voltage is a monotonically increasing function of a (i.e., a, b are coefficients of bistable potential) and monotonically decreasing function b for a given set of parameters.
(3) At low value of noise intensity, the joint PDF shows two sharp isolated larger peaks, and the corresponding contour plot reveals that it almost behaves like a deterministic oscillator. As the noise intensity increases sharply, the bimodal peaks tend to flatten and begin to merge, i.e., the nonlinear interaction between the oscillator and the stochastic excitation increases and jump of system response from one potential well to another is also observed in the corresponding contour plot. Similar phenomena are observed in case of viscous damping.
(4) Mean square value of output voltage increases as noise intensity increases and decreases at higher values of viscous damping.
(5) Output power of the BEH increases with larger values of time constants.

This method can also be applied to micro- and nanomechanical resonators where Gaussian white noise-driven dynamics are considered as a promising option.

Compliance with Ethical Standards

Funding This research received no specific grant from any funding agency in the public, commercial or not-for-profit sectors.

Conflict of interest The authors declare no conflict of interest in preparing this article.

Appendix

$$
\begin{aligned}
E\left[x^2\right] = \left\langle x^2 \right\rangle &= \int_{-\infty}^{\infty}\int_{-\infty}^{\infty} x^2 P_{st}\left(x, y\right) \mathrm{d}x\mathrm{d}y \\
&= \int_{-\infty}^{\infty} x^2 P_{st}\left(x\right) \mathrm{d}x \int_{-\infty}^{\infty} A_2 \exp\left(-\frac{\gamma}{2D} y^2\right) \mathrm{d}y \\
&= \int_{-\infty}^{\infty} x^2 P_{st}\left(x\right) \mathrm{d}x \\
&= \int_{-\infty}^{\infty} x^2 \exp\left[-\frac{\gamma}{D}\left(-\frac{1}{2}\left(a + \kappa_v \kappa_c\right) x^2 + \frac{1}{4} b x^4\right)\right] \mathrm{d}x \\
&= \int_{-\infty}^{\infty} x^2 \exp\left[-A\left(x^2 + B x^4\right)\right] \mathrm{d}x \\
&= \frac{\sqrt[4]{\frac{A}{B}} \exp\left(\frac{A}{8B}\right)}{8B\sqrt[4]{AB}} \left[K_{3/4}\left(\frac{A}{8B}\right) - K_{1/4}\left(\frac{A}{8B}\right)\right]
\end{aligned}
$$

where $A = -\frac{\gamma\left(a+\kappa_v\kappa_c\right)}{2D}$, $B = -\frac{b}{2\left(a+\kappa_v\kappa_c\right)}$ and $K_\nu\left(z\right)$ is Bessel function of the second kind and ν order [19].

References

1. Anton, S.R.; Sodano, H.A.: A review of power harvesting using piezoelectric materials. Smart Mater. Struct. **16**, 1–229 (2007)
2. Priya, S.: Advances in energy harvesting using low profile piezoelectric transducers. J. Electroceram. **1**, 165–167 (2007)
3. Stephen, N.G.: On energy harvesting from ambient vibration. J. Sound Vib. **293**, 409–425 (2006)
4. Williams, C.B.; Yates, R.B.: Analysis of a micro-electric generator for micro-systems. Sens. Actuators Appl. Phys. **52**, 8–11 (1996)
5. Glynne-Jones, P.; Tudor, M.J.; Beeby, S.P.: White NM An electromagnetic vibration powered generator for intelligent sensor systems. Sens. Actuators A Phys. **110**, 344–349 (2004)
6. Tvedt, L.G.W.; Nguyen, D.S.; Halvorsen, E.: Nonlinear behavior of an electrostatic energy harvester under wide-and narrowband excitation. J. Microelectromech. Syst. **19**, 305–316 (2010)
7. Roundy, S.; Wright, P.K.: A piezoelectric vibration based generator for wireless electronics. Smart Mater. Struct. **13**, 1131 (2004)
8. Shu, Y.; Lien, I.: Analysis of power output for piezoelectric energy harvesting systems. Smart Mater. Struct. **15**, 1499 (2006)
9. Meninger, S.; Mur-Miranda, J.O.; Amirtharajah, R.; Chandrakasan, A.; Lang, J.: Vibration-to-electric energy conversion. IEEE Trans. Very Large Scale Integr. (VLSI) Syst. **9**, 64 (2001)
10. Cottone, F.; Vocca, H.; Gammaitoni, L.: Nonlinear energy harvesting. Phys. Rev. Lett. **102**, 080601 (2009)
11. Gammaitoni, L.; Neri, I.; Vocca, H.: Nonlinear oscillators for vibration energy harvesting. Appl. Phys. Lett. **94**, 164102 (2009)
12. Ferrari, M.; Ferrari, V.; Guizzetti, M.; Ando, B.; Baglio, S.; Trigona, C.: Improved energy harvesting from wideband vibrations by nonlinear piezoelectric converters. Sens. Actuator Phys. **162**, 425–431 (2010)
13. Erturk, A.; Inman, D.J.: Piezoelectric Energy Harvesting. Wiley, Chichester (2011)
14. Friswell, M.I.; Ali, S.F.; Bilgen, O.; Adhikari, S.; Lees, A.W.; Litak, G.: Non-linear piezoelectric vibration energy harvesting from a vertical cantilever beam with tip mass. J. Intell. Mater. Syst. Struct. **23**, 1505 (2012)
15. Litak, G.; Friswell, M.I.; Adhikari, S.: Magnetopiezoelastic energy harvesting driven by random excitations. Appl. Phys. Lett. **96**, 214103 (2010)
16. Daqaq, M.F.: Transduction of a bi-stable inductive generator driven by white and exponentially correlated Gaussian noise. J. Sound Vib. **330**, 2254–2264 (2011)
17. Kumar, P.; Narayanan, S.; Adhikari, S.; Friswell, M.I.: Fokker-Planck equation analysis of randomly excited nonlinear energy harvester. J. Sound Vib. **333**, 2000–2033 (2014)
18. Zhu, P.: Statistical stationary properties of nonlinear energy harvesting system under high-pass filter. Chin. J. Phys. **54**, 545–554 (2016)
19. McLachan, N.W.: Bessel Functions for Engineers. Clarendon Press, Oxford (1934)